PHYSICAL REVIEW B **93**, 094102 (2016)

Identification of the specific Fe centers and associated defect structure responsible for enhanced dynamic holography in photorefractive $KNbO_3$:Fe

S. A. Basun[1,2] and D. R. Evans[1,*]
[1]*Air Force Research Laboratory, Materials and Manufacturing Directorate, Wright-Patterson Air Force Base, Ohio 45433, USA*
[2]*Azimuth Corporation, 4134 Linden Avenue, Suite 300, Dayton, Ohio 45431, USA*

(Received 20 July 2015; revised manuscript received 22 December 2015; published 10 March 2016)

A multifaceted approach is used to identify the Fe centers associated with $KNbO_3$:Fe, determine the location of energy levels, and conclude which centers play a vital role in the photorefractive effect; with such an understanding, the physical parameters may be modified to provide mature materials for dynamic holographic applications. A correlated study is performed on as-grown and reduced $KNbO_3$:Fe crystals, where a uniform reduction is achieved through a modified electroreduction process. This investigation identifies which Fe centers are reduced and which are unaffected, allowing the existence of both charge donors and acceptors as required for photorefraction, resulting in significant improvements of the photorefractive properties. Available charge transitions as a function of photon energy are identified and associated with conditions necessary for major improvements in beam-coupling efficiencies and response times. The understanding of the dynamics and defect structure is supported by photorefractive beam-coupling data. A revised explanation of the photorefractive dynamics is given as this understanding of the defects in $KNbO_3$:Fe is no longer described by the commonly used standard model. This new fundamental understanding that enables the development of improved materials for dynamic holographic applications may also be transferred to other materials classes for disparate applications.

DOI: 10.1103/PhysRevB.93.094102

I. INTRODUCTION

Although advances in the understanding of photorefractive physics and optics have been made over the past couple of decades, the materials themselves have not matured, thus explaining why there is no significant commercial activity using photorefractive materials [1]. Without a fundamental understanding of the required defect structure of these materials and the key roles these defects play in the photorefractive effect, they cannot be optimized for use in particular applications. A detailed understanding of the available centers and the dynamics of charge transfer is still needed. In this paper, attention is focused on obtaining such an understanding in order to engineer a crystal for use in two-beam coupling applications. In particular, this paper focuses on the material properties and charge transfer dynamics in iron-doped potassium niobate ($KNbO_3$:Fe), where lessons learned from this paper may transfer to other materials classes. $KNbO_3$ crystals are attracting a lot of interest in nonlinear optics due to large electro-optic coefficients and high nonlinear optical susceptibilities [2–8], making them suitable materials (if matured) in numerous optical and electro-optical applications. In considering photorefractive beam coupling, Fe-doped $KNbO_3$ samples can provide a dramatic increase in photorefractive sensitivity and speed, which can be achieved through a reduction treatment that converts part of the Fe^{3+} ions in the $KNbO_3$ lattice to the Fe^{2+} valence state [4,9,10]. Despite this progress, significant shortcomings still prevent this material from finding its way to application. To fully mature these materials, it is necessary to have an in-depth understanding of the defect structure, interplay of photoelectron transfer, electron-hole competition, energy transitions responsible for the photorefractive effect, a means of optimizing the donor and acceptor concentrations, and even the knowledge of what centers actually play the role of charge donor and acceptors (as a function of reduction, beam-coupling wavelengths, etc.).

In a simple, yet reasonable, model such as the one used to describe the photorefractive effect in $LiNbO_3$:Fe [4], when under irradiation in the visible, Fe^{2+} ions serve as a source of photoelectrons, and Fe^{3+} ions are electron traps. In the presence of an optical interference pattern, these charge donors and acceptors are responsible for the creation of a periodic space-charge electric field and in turn a photorefractive grating. Since the Fe ions need to exist presumably as Fe^{2+} and Fe^{3+} to generate the photorefractive effect, a means to control the mixture of the valence states of Fe without going through multiple phase changes during annealing is required. Unlike $LiNbO_3$:Fe, $KNbO_3$:Fe undergoes numerous phase changes, making the common annealing process for Fe reduction impractical. Passing through multiple phase changes would damage the crystal. A common and practical method is electroreduction (a field-assisted diffusion of impurities), which converts the Fe^{3+}-dominated as-grown crystal into one with both charge donors and charge acceptors (i.e. mixed valence states). Although uniformity and reproducibility are issues in reduced crystals, the dynamic holographic performance (e.g. as in photorefractive beam-coupling experiments) can be dramatically improved. A detailed understanding of the role of the defect structure in $KNbO_3$:Fe, as a result of both growth and postgrowth treatments, may provide opportunities for further improvements to this promising material. Furthermore, a new level of understanding of the role of various centers and complexes in $KNbO_3$ may extend to multiple classes of materials that would allow them to be tailored for disparate applications, e.g. image processing, image broadcasting, edge enhancement, optical storage, phase conjugation, and holographic displays, etc. [11–16]. With advanced materials, such as the improved $KNbO_3$:Fe, these applications may become practical [17]. The understanding achieved through this paper demonstrates the importance of a deep knowledge of the defect structure in

---

[*] Corresponding author: dean.evans@us.af.mil

2469-9950/2016/93(9)/094102(12)

order to make significant improvements to material properties for improved performance in applications.

Fe^{3+} centers in $KNbO_3$ were studied in a number of publications [4,18–23]. Several types of Fe^{3+} centers have been considered: $Fe^{3+}[Nb^{5+}]$ (isolated Fe^{3+} ion that substitutes for Nb^{5+} in the oxygen octahedron) [19–21], $Fe^{3+}[Nb^{5+}]$-V_O (Fe^{3+} ion that substitutes for the Nb^{5+} with a neighboring oxygen vacancy) [19,21], and $Fe^{3+}[K^+]$-V_K (Fe^{3+} ion that substitutes for K^+, with a K vacancy in the first coordination shell of the K ions) [19]. Several other complexes with unidentified defects adjacent to $Fe^{3+}[Nb^{5+}]$ have also been reported [22]. Despite the variety of Fe centers in $KNbO_3$, the specific Fe center responsible for the photorefractive effect (charge donors and charge acceptors) has not been previously identified.

The main goal of this paper is to determine which specific Fe centers are responsible for the enhanced photorefractive effect and, more specifically, how the growth process or the postgrowth electroreduction process could be tailored to increase the concentration of the necessary defect structure for particular applications (e.g. providing a uniform distribution of both donors and acceptors, as required for the photorefractive effect in dynamical holographic applications). For the first time, a study of Fe associated defects is presented comparing as-grown (unreduced) and reduced $KNbO_3$:Fe and providing relative concentrations of the Fe centers responsible for the various charge transitions that play a role in the photorefractive effect. This is achieved by correlated studies of electron paramagnetic resonance (EPR) and optical absorption spectra of as-grown (poled, unreduced) and electroreduced samples, which allow for the identification of a specific complex center as the *main* photorefractive center in $KNbO_3$:Fe. It is the complex that allows for an increase of the electron donor concentration in the donor-starved as-grown crystals which leads to an enhanced performance of photorefractive two-beam coupling with an increased gain coefficient, reduced response time, and minimized electron-hole competition. The need for an oxygen-free environment is stressed in this paper, and in addition to the gas used for reduction, the importance of electrode material is demonstrated resulting in a *uniform* reduction. Furthermore, from dark conductivity and optical absorption spectra, the energy level positions in the bandgap are determined, and the particular energy transitions of the Fe centers in both as-grown and reduced $KNbO_3$:Fe crystals resulting in hole, electron, or competing photorefractive processes are identified. Finally, it will be shown that only one of several Fe species undergoes reduction; this insight may provide a means to improve material properties and tailor the crystal for various electro-optic/photorefractive applications.

II. EXPERIMENTAL

$KNbO_3$:Fe crystals (2000 ppm of Fe in the melt) were provided by VLOC (Trinity, FL). For the results in Secs. III A through III D, the samples were cut from the same boule and were approximately 3 mm cubes with the faces orthogonal to the *a*, *b*, and *c* crystallographic axes. The *c* and *b* faces were polished to optical and inspection quality, respectively. To obtain single domain crystals, the samples were poled at 180 °C by applying 500 V across the *c* faces that were coated with electrodes. As soon as poling occurred (viewed through the *b* faces), which was approximately a minute, the voltage was removed, and the samples were cooled down to room temperature. Such a procedure (a short exposure to an electric field) resulted in a single domain character of the crystals, it did not change other material properties, i.e. no reduction occurred; color of the samples remained a yellowish green. The electrodes were removed from the *c* faces in order to measure the optical absorption spectra, the EPR spectra, and the dynamic holographic performance (via two-beam coupling measurements).

Several methods of reduction for bulk $KNbO_3$ samples are known: (1) high temperature annealing in a reducing or oxygen-deficient atmosphere (Refs. [4,24]), (2) prolonged application of an electric field at moderately elevated temperature (electroreduction, i.e. field-assisted diffusion/indiffusion [3,10,24–28]), and (3) substituents (e.g. Ag and Rb) in the K-site, in the melt, resulting in a recharging of the photorefractive center in the Nb site (i.e. Fe, Ni) [5,17,29]. For this paper, the second method was employed in order to avoid many of the complications associated with heating above the orthorhombic-tetragonal phase transition temperature (218 and 203 °C upon heating and cooling, respectively [4,30,31]). As demonstrated in this paper, this method is not only affected by atmosphere, temperature, and electric field; it also strongly depends on the electrode material. Method (2) was specifically chosen to overcome the inhomogeneity of reduction, i.e. the primary problem with method (3). This reduction procedure is practically the same as the previously described domain poling, with the main difference being in the time period in which the voltage was applied at 180 °C (7 days). Various electric contact materials were deposited onto the *c* faces to check for effects of the electrode material, i.e. silver or gold paints, silver or gold metal films, and carbon (Aquadag®). It is worth noting that the use of the term "as-grown" throughout this paper refers to crystals that have been rapidly poled, but not reduced. The term "reduced" refers to poled samples that have been subjected to a prolonged electroreduction process (i.e. a field-assisted diffusion process).

Electron paramagnetic resonance spectra of a series of as-grown and reduced samples were measured with a Bruker EMX EPR spectrometer equipped with a standard resonator ER 4102ST operating near 9.7 GHz. With such small samples (3 mm cubes), no significant effect on the Q value of the resonator occurred. Because of the highly anisotropic character of the spectra (typical of the axial Fe^{3+} centers), a complete set of angular dependencies was taken in the *ac*, *ab*, and *bc* crystallographic planes with an increment of 5°. Parameters of the spin-Hamiltonians to fit the angular dependencies were found with an EPR-NMR software package [Computer Program EPR–NMR (Department of Chemistry, University of Saskatchewan, Canada, 1993)].

Optical transmission spectra were taken with a Cary 5000 spectrophotometer on the same series of crystals used for the EPR measurements, comparing the difference in the absorption spectra between the as-grown and electroreduced samples. The light was propagated along the *c* axis of the samples, and the spectra were corrected for Fresnel reflections using Sellmeier equations [32].

Electric conductivity as a function of temperature was measured with a nitrogen gas flow cryostat. The *a* faces of the samples were coated with carbon, and the current was approximately proportional to the applied voltage. Voltage of 100–300 V was applied across the *a* faces, which strongly suppressed unwanted contributions of pyroelectric current caused by inevitable minor temperature fluctuations. The temperature range of the measurements was limited by the orthorhombic-to-rhombohedral phase transition at ∼−10 °C and the orthorhombic-to-tetragonal phase transition at ∼210 °C.

The evaluation of the dynamic holographic performance was achieved by measuring the dynamics of two-beam coupling in a nonuniformly reduced crystal, with both unreduced (i.e. as-grown) and reduced regions. This individual crystal containing both regions was purposely chosen to avoid potential variations that can occur from sample to sample. The sample ($4\times8\times7\ \mathrm{mm}^3$ along the x,y, and z axes, respectively) had regions of either a yellowish-green color or a brownish color, typical of as-grown and reduced crystals, respectively. Two-beam coupling was achieved using a continuous wave (CW) 532 nm Verdi laser in a self-pumped reflection geometry [33]. The key parameters in this evaluation, the photorefractive response times, two-beam coupling efficiencies, and the sign of the charge carriers (determined by the direction of gain with respect to the $+c$ axis and the sign of the electro-optic coefficients), were measured by monitoring the transmitted beam in a counter-propagating self-pumped reflection geometry in both unreduced and reduced regions of the crystal.

III. RESULTS

The Results section is divided into six parts. In Secs. A and B, different Fe centers are identified in as-grown and reduced $\mathrm{KNbO_3}$:Fe, as well as their change in concentration as a result of reduction. In Secs. C, D, and E, electrical and optical methods are employed to determine the energy level positions in the bandgap and identify electron/hole transitions over a broad spectral region that play a role in space-charge field generation (i.e. photorefractive effect) in as-grown and reduced samples. Specifically, in Sec. E, the interplay of hole and electron transitions over three distinct photon energy regions in both as-grown and reduced crystals is described in terms of the enhancement or competing processes in the formation of photorefractive gratings. Finally, in Sec. F, photorefractive beam coupling is compared in unreduced and reduced regions in the same nonuniformly reduced crystal, where only the centers identified as the main photorefractive centers are considered in order to establish the effects of “pure-hole” and “pure-electron” processes in dynamic holographic applications. We show a dramatic improvement of the strength of the space-charge field and speed in the formation of the photorefractive grating as a result of the type of the photo-generated charge carriers.

A. EPR of Fe-related centers in $\mathrm{KNbO_3}$

Electron paramagnetic resonance is a useful technique for determining the types of impurities in a single crystal and their locations within the host lattice. Electron paramagnetic resonance spectra of $\mathrm{KNbO_3}$:Fe are well described by the following spin-Hamiltonian with an isotropic g factor [18,19]:

$$H=\sum_{m=-2}^{2} hB_2^m O_2^m+\sum_{m=-4}^{4} hB_4^m O_4^m+g\beta S\cdot B, \qquad (1)$$

where the crystal spin operators O_n^m are linear combinations of tensor operators, B_n^m are coefficients, h is Planck’s constant, and the third term of the Hamiltonian is the electron spin term [34]. All the resonances found in the angular dependencies of the EPR spectra for all of our samples are split into two sets of spin-Hamiltonian parameters. Although the spin-Hamiltonian parameters are the same for the as-grown and reduced samples, there is a difference in the amplitudes of the resonances. The ratio of the concentrations of these isolated centers and complex centers is strongly dependent on the level of reduction, where “isolated centers” are defined as isolated Fe ions and “complex centers” are defined as Fe ions with a neighboring defect. All of the parameters for our samples are given in Table I, along with previously published results found in Refs. [19–21].

In all the studies, including this paper, the center with $B_2^0\approx1.8$ GHz (i.e. zero field splitting, the most important parameter) was ascribed to $\mathrm{Fe^{3+}}$ substitutional for $\mathrm{Nb^{5+}}$ without local charge compensation, $\mathrm{Fe^{3+}[Nb^{5+}]}$ center. The main axis of this center is along the pseudocubic b axis of the orthorhombic phase, and the point symmetry group of the center is C_{2v}.

The situation with Fe centers other than $\mathrm{Fe^{3+}[Nb]}$ is much less clear. No centers other than $\mathrm{Fe^{3+}[Nb]}$ were found in Ref. [20], but Refs. [19,21] reported on the presence of an additional axial $\mathrm{Fe^{3+}}$ center in their samples (see Table I). The two most probable cases were pointed out by Siegel *et al.* (K. A. Müller Group) in Ref. [19] as either $\mathrm{Fe^{3+}[K]}$-V_K ($\mathrm{Fe^{3+}}$ on $\mathrm{K^+}$ site with an adjacent potassium vacancy) or $\mathrm{Fe^{3+}[Nb]}$-V_O ($\mathrm{Fe^{3+}}$ on $\mathrm{Nb^{5+}}$ site with an adjacent oxygen vacancy) complexes. In Ref. [19], Siegel *et al.* noted that the B_2^0 value of their $\mathrm{Fe^{3+}}$ center was only half the value of the $\mathrm{Fe^{3+}}$-V_O center in $\mathrm{SrTiO_3}$ and $\mathrm{KTaO_3}$, “and thus it is not sure whether it is of this nature.” A similar comment was made by Possenriede *et al.* (O. F. Schirmer Group) in Ref. [21] that the center with $B_2^0=7.3$ GHz (Ref. [19]) could be excluded from being $\mathrm{Fe^{3+}}$-V_O because of its small B_2^0.

The value of $B_2^0=11.5$ GHz reported by Possenriede *et al.* in Ref. [21] for the $\mathrm{Fe^{3+}}$ complex center, which is significantly larger than the value found by Siegel *et al.* in Ref. [19] ($B_2^0=7.3$ GHz), allowed the authors of Ref. [21] to assign their center to $\mathrm{Fe^{3+}[Nb]}$-V_O. Possenriede *et al.* showed positions of the resonances in the EPR spectra and the angular dependence of the $\mathrm{Fe^{3+}}$ complex center, which appear practically identical to those measured in this paper for the $\mathrm{Fe^{3+}}$ complex center at a similar microwave frequency, strongly suggesting the same nature of the centers.

Considering the significant difference in the B_2^0 values of the $\mathrm{Fe^{3+}}$ complex centers found by Possenriede *et al.* [21] with respect to the values obtained in this paper and by Siegel *et al.* [19], it is not unreasonable to ask if these centers are indeed different. The difficulty in addressing such a question is that a straightforward comparison of the EPR spectra does not appear possible: the spectrum provided in Ref. [19] and the angular dependencies (not provided in Ref. [19]) were

TABLE I. Spin-Hamiltonian parameters of Fe^{3+} centers in $KNbO_3$ (from this paper and Refs. [19–21]). The observed centers are the same in our as-grown and reduced samples, although there is a striking difference in the amplitudes of the resonances (see Fig. 1).

Fe^{3+} center	Ref.	g	B_2^0(GHz)	B_2^2(GHz)	B_4^0(GHz)	B_4^2(GHz)	B_4^4(GHz)
Fe^{3+}[Nb]	[19,20]	2.0053 ± 0.0008	$\mp1.779 \pm 0.0007$	$\pm0.293 \pm 0.003$	$\pm0.00283 \pm0.00003$	$\mp0.00115 \pm0.00045$	$\mp0.0122 \pm0.0005$
	[21]	2.0010 ± 0.0020	$\mp1.752 \pm 0.002$	$\pm0.393 \pm 0.06$	±0.00237		$\pm0.0116 \pm 0.0025$
	This paper	1.9984 ± 0.0014	$\mp1.758 \pm 0.002$	$\pm0.294 \pm 0.005$	$\mp0.00022 \pm0.00009$	$\pm0.01285 \pm 0.00033$	$\pm0.0104 \pm 0.0005$
Fe^{3+}[K]-V_K or less likely Fe^{3+}[Nb]-V_O	[19]		$\pm7.3 \pm 0.7$	$\pm1.33 \pm 0.03$	$\mp0.067 \pm 0.017$		
Most likely Fe^{3+}[K]-V_K	This paper	1.995 ± 0.002	$\pm7.17 \pm 0.13$	$\pm1.28 \pm 0.27$	$\pm0.0081 \pm 0.0016$		
Fe^{3+}[Nb]-V_O	[21]	$g_{\mathrm{eff},1} = 1.940 \pm 0.010$ $g_{\mathrm{eff},2} = 7.035 \pm 0.005$ $g_{\mathrm{eff},3} = 4.865 \pm 0.005$	$\pm11.5 \pm 0.5$	1.59 ± 0.15			

taken at a very different microwave frequency (13.9 GHz) than those used in Ref. [21] and in this paper (≈9 GHz). Only the spin-Hamiltonian parameters can be compared.

At this point, attention should be drawn to the fact that different values of B_2^0 for the Fe^{3+} complex centers found by Siegel *et al.* [19] and Possenriede *et al.* [21] (Table I) were obtained in quite different ways. Possenriede *et al.* [21] employed the method suggested by Kirkpatrick *et al.* (K. A. Müller Group) in Ref. [35] of conducting measurements at two microwave frequencies with the assumption of a strongly anisotropic tensor g_{eff} characteristic of Fe^{3+} in a strong axial field; 9 and 34 GHz frequencies were used [21]. Results in Ref. [19] were obtained with the use of the spin-Hamiltonian [Eq. (1)] with an isotropic g factor. Since this paper employs a standard single frequency method to measure the EPR spectra (as done by Siegel *et al.* [19]), we deliberately used the same spin-Hamiltonian and the same choice of nonzero parameters as used in Ref. [19] to process our data; this resulted in a set of parameters of nearly the same values (see Table I), including B_2^0. This makes it highly probable that the complex center in our samples is the same as found by Siegel *et al.* in Ref. [19]). At the same time, based on the close match between the angular dependencies of the resonances in this paper and those provided by Possenriede *et al.* [21], it has been demonstrated above that the complex centers are the same. Thus, the additional center in all three cases (Refs. [19,21], and this paper) must be the same.

In addition to Fe^{3+}[Nb] and Fe^{3+}[Nb]-V_O centers, Ref. [22] reports on the observation of several other Fe centers in $KNbO_3$, viz. Fe^{+}[K], Fe^{3+}[Nb]-X, Fe^{3+}[Nb]-Y, Fe^{3+}[Nb]-Z, and Fe^{3+}[?]. In our samples, there were a few unidentified lines that were a couple of orders of magnitude smaller than the lines of Fe^{3+}[Nb] and Fe^{3+} complex centers. These vanishingly weak lines, as well as the strong lines for the Fe^{3+}[Nb] center showed no dependence on reduction, unlike the resonances of the main complex center (described in Sec. B).

The main goal of this paper was to locate the dominant *photorefractive* Fe centers among all Fe species present in as-grown and reduced $KNbO_3$:Fe, particularly those responsible for increasing the donor center concentration. The aim was to determine the effect that electroreduction has on the charge state of Fe in the complex center compared to the isolated centers that were unaffected, and to establish the influence of the recharged (reduced) complex center on the photorefractive effect in $KNbO_3$:Fe. The focus of this paper was not intended to determine the most sensible set of spin-Hamiltonian parameters for the Fe^{3+} complex center in $KNbO_3$, nor to shed more light on its nature; although the results given below (Sec. B) strongly support the Fe^{3+}[K]-V_K nature of the Fe^{3+} complex center. Furthermore, one must consider that the samples in the previous EPR studies were grown under different conditions and by different growers, which suggests that the defect structure may be affected by the growth or postgrowth procedures. This may account for the different results found in the literature. For the sake of simplicity, in this paper, the following notation is used: Fe^{3+}-V.

B. EPR spectra: Effects of reduction on Fe^{3+}[Nb] and Fe^{3+}-V centers

Portions of the EPR spectra collected on the as-grown and reduced samples are shown in Fig. 1 [traces (a) and (b), respectively]. At the microwave frequency of 9.7 GHz, EPR spectra of Fe^{3+}[Nb] are rather complicated, having a large number of resonances caused by the small value of B_2^0 with respect to the microwave frequency. With the magnetic field parallel to the *a* axis, the strongest resonance is at 3768 G, while the other lines are significantly weaker. A larger B_2^0 value of Fe^{3+}-V simplifies the spectrum: only two lines of Fe^{3+}-V are in Fig. 1 at 2069 G [the strongest line in Fig. 1(a) in an as-grown sample] and 1541 G.

The EPR spectra in Fig. 1 led to two important conclusions: (1) Fe^{3+}[Nb] is not a dominant Fe^{3+} center in as-grown $KNbO_3$:Fe crystals as the concentration of Fe^{3+}-V appears quite comparable or even larger than that of Fe^{3+}[Nb] [Fig. 1(a)], and (2) a comparison of the spectra of the as-grown and reduced samples [Figs. 1(a) vs 1(b)] shows

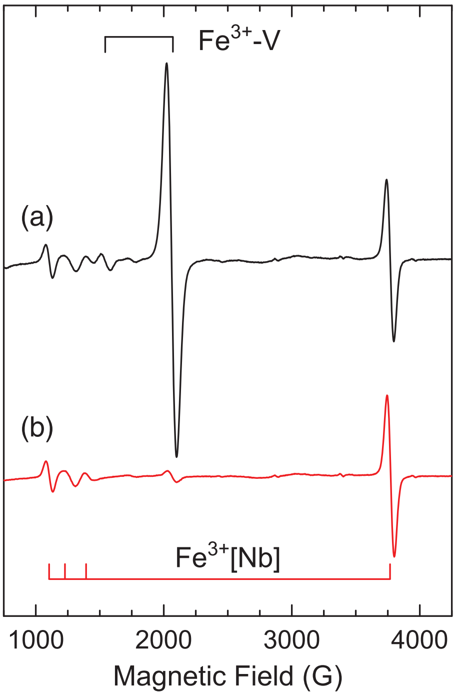

FIG. 1. Portions of the EPR spectra of KNbO$_3$:Fe: (a) a poled as-grown crystal, and (b) a reduced sample via electroreduction with gold paint electrodes. Positions of the resonances from Fe^{3+}-V and Fe^{3+}[Nb] indicated (top and bottom, respectively). Magnetic field parallel to the *a* axis, microwave frequency 9.7 GHz.

that reduction causes a dramatic decrease of the concentration of Fe^{3+}-V (a factor of 30, using gold paint electrodes for electroreduction), while the concentration of Fe^{3+}[Nb] remains unaffected. Gold metal electrodes have a similar effect as gold paint. Electroreduction with the silver paint, silver metal, and carbon electrodes results in a smaller decrease of the Fe^{3+}-V concentration (a factor of 3–4). This is consistent with Refs. [3,24], where electroreduction in oxygen-deficient atmospheres produces stronger changes than with ambient air, pointing to the principal role of oxygen vacancies [4]. In this paper, the effect of a nonoxidizing environment by using nonoxidizing metal electrodes (Au) in air was explored. The use of Au produced stronger reduction (10×) compared to other electrode materials, as well as a significant improvement to the uniformity of the reduction (i.e. uniform absorption).

Although the EPR results show evidence of Fe^{3+} with an adjacent vacancy (Fe^{3+}-V), the results do not support the presence of Fe^{3+}[Nb^{5+}]-V_O complexes. While there is evidence of V_O playing an essential role in the electroreduction process, it does not necessarily imply that they form complexes with Fe^{3+} (i.e. of Fe^{3+}-V_O). As it is *neutral* oxygen (O) that leaves the crystal as a result of a field-assisted diffusion, two electrons that were previously bound by oxygen as a host ion (O^{2-}) remain. These electrons minimize their potential energy when they become captured by the deepest available empty defects, thus reducing their charge (valence) state (for example: $e^- + \mathrm{Fe}^{3+} \rightarrow \mathrm{Fe}^{2+}$). Aggregation of oxygen vacancies with Fe^{3+}[Nb] (formation of Fe[Nb]-V_O complex) in the course of reduction would certainly cause a decrease in the Fe^{3+}[Nb] concentration. On the contrary, an opposite behavior is observed: the Fe^{3+}[Nb] concentration remains unchanged. Figure 1 shows clear evidence (note the resonance at 3768 G is unchanged by reduction) that such an effect is insignificant if not completely absent. This supports the Fe^{3+}[K]-V_K nature of the Fe^{3+} complex center, rather than Fe^{3+}[Nb]-V_O, despite the formation of oxygen vacancies (V_O).

The process of reduction in KNbO$_3$:Fe is illustrated in Ref. [4] by the energy level diagram for Fe centers in the bandgap of KNbO$_3$ (without any use of complex Fe centers), this was used in order to explain various photorefractive properties of KNbO$_3$:Fe (Figs. 7.7 and 7.19 in Ref. [4]). According to Zgonik *et al.* (P. Günter Group) in Ref. [4], isolated Fe can exist in KNbO$_3$ in one of the three charge states: Fe^{4+},Fe^{3+}, and Fe^{2+} (Fe^{3+}/Fe^{4+} and Fe^{2+}/Fe^{3+} levels in the bandgap, where the Fe^{3+}/Fe^{4+} is the lowest level). In the explanation provided in Ref. [4], the Fe^{2+}/Fe^{3+} levels are empty in an unreduced sample (Fe^{2+} ions are absent), while Fe^{3+}/Fe^{4+} levels are partially filled with electrons, allowing the presence of both Fe^{3+} and Fe^{4+} with the Fermi level pinned to the Fe^{3+}/Fe^{4+} level. The removal of oxygen and the associated increase in unbound electrons gradually fills in the Fe^{3+}/Fe^{4+} level (this increases the concentration of Fe^{3+} and simultaneously decreases that of Fe^{4+}). In a partially reduced sample at a certain stage of reduction, all Fe^{3+}/Fe^{4+} levels become filled with electrons (Fe^{4+} disappears, only Fe^{3+} and Fe^{2+} charge states remain), and subsequently, the filling of the Fe^{2+}/Fe^{3+} levels begins, thus pinning the Fermi level to the Fe^{2+}/Fe^{3+} level. Further removal of oxygen results in more electrons to be readily available to fill the Fe^{2+}/Fe^{3+} level, thus increasing the concentration of Fe^{2+} with a simultaneous decrease of Fe^{3+}. According to the common point of view given in Ref. [4], it is the increase of the concentration of isolated Fe^{2+} (accompanied by the corresponding decrease of the isolated Fe^{3+} concentration) that causes a strong improvement of holographic performance of KNbO$_3$:Fe.

In a clear contrast to the above-stated viewpoint, the EPR results in Fig. 1 show comparable concentrations of Fe^{3+}-V (2069 G) and Fe^{3+}[Nb] (3768 G) lines in the as-grown samples. Upon reduction, there is a strong decrease of the Fe^{3+}-V concentration with no change to that of isolated Fe^{3+}[Nb]. This causes a need in a modification to the above-described model of just one center (isolated Fe) that can exist in KNbO$_3$ in three different charge states. The correspondingly modified energy level diagram is shown in Fig. 2 and will be widely used throughout this paper. Our version of the energy level diagram is drawn in a similar manner as Figs. 7.7 and 7.19, and Table 7.5 in Ref. [4], which follows the Born-Haber cycle [36]. The required major change to the diagram was to replace the upper level (Fe^{2+}/Fe^{3+}) in the bandgap with Fe$^{2+/3+}$-V. With this change, the decrease of the Fe^{3+}-V concentration observed in EPR is explained by the reduction of the centers to their EPR silent charge state, Fe^{2+}-V (i.e. an even number of electrons in Fe^{2+} with a $3d^6$ electron configuration). The reason for the reduction of Fe^{3+}-V and no reduction of Fe^{3+}[Nb] is simply the change in the position of the Fermi level in reduced samples (Fig. 2). As shown below, it is the increase of the Fe^{2+}-V concentration upon reduction that brings a strong improvement to photorefractive properties and modifies the optical absorption and electric conductivity of KNbO$_3$:Fe. The positions of the Fe levels in the bandgap of

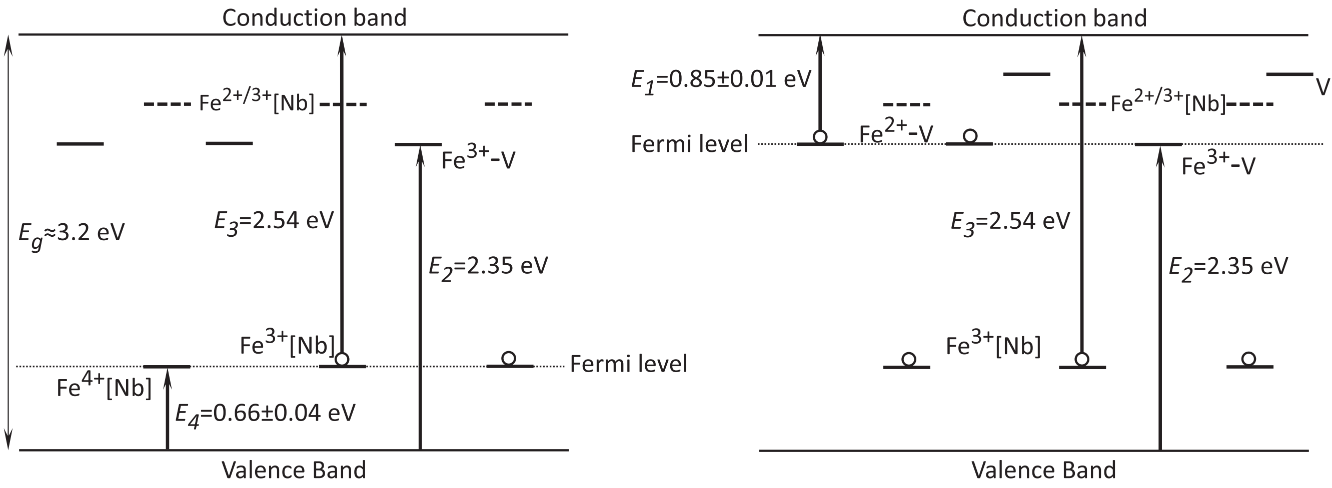

FIG. 2. Schematics of the energy levels of different defect centers (Fe-V, Fe[Nb], and V_O) in the bandgap of $KNbO_3$, drawn in the spirit of Figs. 7.7 and 7.19 in Ref. [4]. Only "thermal levels" are shown and drawn as either empty (horizontal bars) or filled with electron (horizontal bars with circles). Left: unreduced (as-grown) sample. Right: reduced sample. Two of the centers shown are taken from Refs. [4,52]: V_O and $Fe^{2+/3+}$[Nb]. The dashed bars represent the $Fe^{2+/3+}$[Nb] levels postulated in Ref. [4].

$KNbO_3$:Fe found in Refs. [4,37] obtained using a holographic method are further refined through our *direct* measurements of the electric conductivity activation energies on as-grown and reduced samples.

Energy level diagrams for Fe in $KNbO_3$ are also given in Refs. [22,38]. Although they are not exactly the same as in Ref. [4], all of the schemes are identical in the following sense: they all consider just *one* Fe center in *three* charge states in $KNbO_3$:Fe. This is completely different from Fig. 2, which has *two* different centers in *two* charge states each, as determined by our EPR results (Sec. A). This is one of the major findings, which is described in detail in this paper, that forced us to revisit the whole picture of $KNbO_3$:Fe under reduction and optical excitation.

It should also be noted that, for the sake of simplicity, only "thermal levels" are shown in Fig. 2. Their location with respect to the host bands determines the energy thresholds (onsets) of the photoelectron transfer transitions, one of the focus points of this paper. The maxima of the corresponding absorption bands are usually located at significantly higher energies (Franck-Condon principle and density of states in a host band) in the case of the "optical levels" approach. Further explanation and examples can be seen in Ref. [23] and references therein. For a better comparison to previously published work on $KNbO_3$:Fe (Refs. [4,22,38]), thermal levels are provided in Fig. 2.

C. Electric conductivity of $KNbO_3$:Fe

Temperature dependence of dc electric conductivity (Arrhenius plot) of as-grown and reduced samples is shown in Fig. 3. A strong increase of conductivity (although still a good insulator, $\sigma < 10^{-10}\ \Omega^{-1}\,\mathrm{m}^{-1}$ at room temperature) in the reduced samples is exactly what is expected from the energy level scheme in Fig. 2, where reduction causes recharging of Fe^{3+}-V to Fe^{2+}-V and thus enables thermal ionization of an electron from Fe^{2+}-V to the conduction band (CB), transition 1(E_1) in Fig. 2. The corresponding activation energy (E_1), 0.85 ± 0.01 eV (the separation between $Fe^{2+/3+}$-V and the CB), found in our direct measurements of dark conductivity is within the error bars of the holographically measured value (indirect measurement of conductivity) provided in Refs. [4,37] for $Fe^{2+/3+}$ (1.0 ± 0.2 eV); this practically coincides with the activation energy of thermal decay of the gratings recorded in 1% Fe-doped $KNbO_3$, 0.81 ± 0.05 eV (Ref. [39]). A quite different activation energy of 1 eV (1.04 ± 0.02 eV in the pure $KNbO_3$) was assigned in Ref. [39] to ionic motion. When considering the error bars for these activation energies, it is evident that the assignments made in Refs. [4,37] and in this

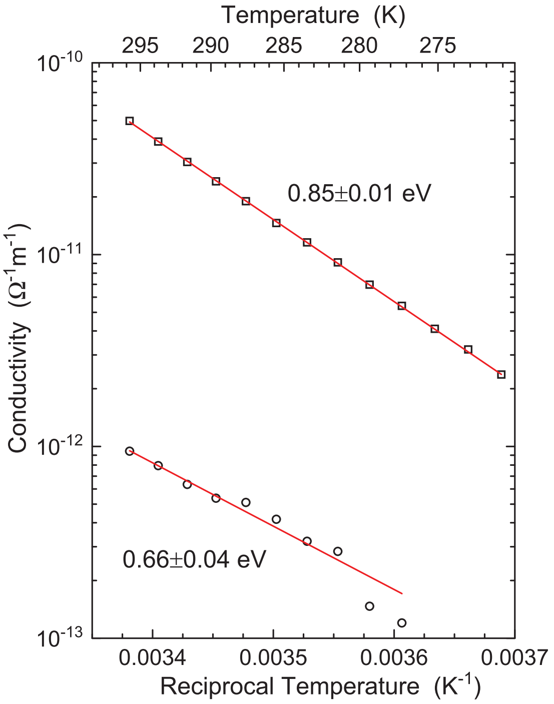

FIG. 3. Electric dark conductivity of the as-grown (circles) and reduced (squares) samples of $KNbO_3$:Fe. Straight lines: fits with $\exp(-\Delta E/kT)$. Activation energies (ΔE) are indicated.

paper are not the same as the activation energy attributed to ionic motion.

In materials similar to $KNbO_3$, the above measured values may be affected by hopping transport of small polarons. The corresponding activation energy for $KNbO_3$ was found to be 0.14 ± 0.05 eV (Ref. [22]) which is very different from any of the values provided in this section. Here, it is necessary to keep in mind that, in Ref. [22], the results were obtained by measuring the decay of *nonequilibrium* charge carriers (on a submicrosecond timescale) generated by a nanosecond pulse irradiation. Dark conductivity, on the contrary, is governed by *equilibrium* carriers: electrons, polarons, and Fe^{2+}-V centers (reduced samples) coexist, and in the dark, they are in thermal equilibrium. Thus, the activation energies presented in this paper and in Refs. [4,37,39] should be attributed to the positions of the Fermi level as seen in Fig. 2.

As-grown (unreduced) samples did not have $Fe^{2+/3+}$-V levels populated; only Fe^{3+}-V complexes were available; thus, transition 1 (E_1, ionization of Fe^{2+}-V) simply could not occur and contribute to conductivity. Instead, there were Fe^{4+}[Nb] ions present (as the $Fe^{3+/4+}$[Nb] levels were populated only partially) that could accept a thermally excited electron from the valence band (VB) leaving a hole in the VB [transition 4(E_4) in Fig. 2]. Our direct measurements of conductivity on as-grown samples (Fig. 3) for transition 4 give an activation energy (E_4) of 0.66 ± 0.04 eV, which is the separation between the VB and $Fe^{3+/4+}$[Nb] level. This value falls within the error bars of the previously reported value of 0.8 ± 0.3 eV in Ref. [4], which was obtained through holographic experiments.

With the measured values of E_1, E_4, and the known bandgap of $KNbO_3$ (E_g), one could straightforwardly obtain threshold energies of the other two transitions in Fig. 2 (E_2 and E_3). Using the Born-Haber cycle, the E_2 and E_3 energies are given by the following equations: $E_2 = E_g - E_1$ and $E_3 = E_g - E_4$. Here, E_g is a "thermal bandgap", the energy separation between the CB minimum and the VB maximum, regardless of the corresponding k-vectors. In optical absorption, the thermal bandgap corresponds to the onset of the fundamental absorption edge; therefore, it is obviously smaller than the "optical bandgap" of $KNbO_3$. In Ref. [31], the "optical bandgap" is defined as the photon energy where the absorption coefficient equals $100\,cm^{-1}$ (at 3.3 eV); when using Tauc plots (Ref. [40]) for direct and indirect bandgaps with our absorption data for undoped $KNbO_3$ (which are in agreement with Ref. [31]), we obtain an average value of the thermal bandgap, $E_g \approx 3.2$ eV. There is only a difference of 0.01 eV between direct and indirect bandgap estimations. For this paper, the thermal bandgap energy value of 3.2 eV will be used. The threshold energies for transitions 2 and 3 (using the values obtained the thermal conductivity results) are estimated as $3.2\text{-}0.85 = 2.35$ eV and $3.2\text{-}0.66 = 2.54$ eV, respectively. Electron transitions 2 and 3 with such high activation energies are not expected to play a role under thermal excitation around room temperature, and dark conductivity is only due to transitions 1 and 4 (reduced and as-grown samples, respectively). Moreover, by determining the activation energies of all Fe centers, it becomes clear why Fe^{3+}-V reduces, while the filled deeper center (Fe^{3+}) does not. Manifestations of all 4 transitions in optical and photorefractive properties, for the reduced and as-grown (unreduced) samples, are considered in the following sections.

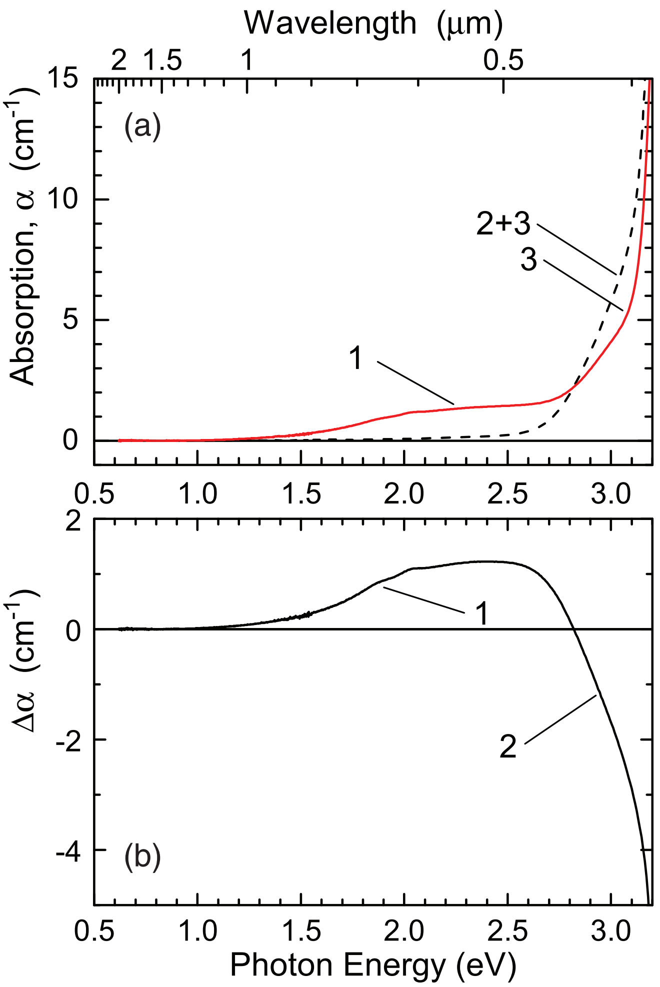

FIG. 4. (a) $KNbO_3$:Fe optical absorption spectra of the as-grown crystal (dashed line) and the same crystal after being reduced (red solid line). Propagation direction c, polarization $E \| b$. (b) Reduction-induced change to the optical absorption $\Delta\alpha$. Assignment of the absorption bands is given in accordance with the electron transitions indicated in Fig. 2.

D. Optical absorption of as-grown and reduced $KNbO_3$:Fe

The observed decrease of the Fe^{3+}-V concentration upon reduction (EPR results, Fig. 1) appears well correlated with the reduction-induced changes to the optical absorption spectra (Fig. 4). Similarly to the EPR spectra, the most pronounced changes were observed with the use of gold electrodes, as shown in Fig. 4. The effect of the silver and carbon electrodes was qualitatively the same but weaker.

Absorption spectra in Fig. 4(a) are consistent with those available in the literature on $KNbO_3$:Fe [4], except with more pronounced effects of reduction; this is similar to the well-studied absorption spectra of $LiNbO_3$:Fe [41,42]. The absorption of as-grown $KNbO_3$:Fe shown in Fig. 4(a) (dashed line) is very weak in the visible and steeply rises in the near ultraviolet (UV). Reduction of the samples [Fig. 4(a), red solid line] gives rise to a very broad absorption band with an onset of ≈0.83 eV that spans from near infrared (IR) to near UV. Analogous to $LiNbO_3$:Fe [41,42], this increase of the absorption in $KNbO_3$:Fe is commonly ascribed to Fe^{2+} ions that are absent in unreduced (as-grown) samples, but appear in the course of reduction treatment converting part of Fe^{3+} ions to the required charge donor Fe^{2+} ions for the photorefractive effect throughout the visible spectrum. The EPR data in Fig. 1 show an unexpected result that the concentration of Fe^{3+}[Nb] ions remains practically unchanged, while the Fe^{3+}-V centers concentration decreases with reduction. Then the correspondingly rising concentration of Fe^{2+}-V must be the cause of the increasing broadband absorption and in turn an improved photorefractive performance due to an increased charge donor concentration. The increasing broadband absorption of $KNbO_3$:Fe due to Fe^{2+}-V (Fig. 4) shows a similar energy position to isolated Fe^{2+} in $LiNbO_3$:Fe (Refs. [42,43]) as well as the Fe^{2+}[Ta]-V_O defect absorption in $KTaO_3$:Fe (Ref. [44]).

The clear correlation between the rising absorption in the visible and strong improvement of photorefractive properties of $KNbO_3$:Fe is supporting evidence that the absorption mechanism is not an intraion transition on an Fe-complex, rather a phototransfer of an electron between the Fe complex and the host electron band. Based on the close similarity of the absorption of Fe^{2+}-V in $KNbO_3$ with the absorption of Fe^{2+}[Nb] in $LiNbO_3$:Fe, the absorption band that rises upon reduction in $KNbO_3$:Fe should be associated with photoinduced electron transfer from Fe^{2+}-V to the CB. This type of photoelectron transfer is often called "photoionization".

In addition to the absorption bands shown in Fig. 4, there is also a strongly polarized ($E\|c$) reduction-induced band in the near IR centered at 1170 nm with a long-wavelength onset of ≈1500 nm (≈0.83 eV) (Ref. [4] and our data, not shown on Fig. 4). The band was attributed to an intraion transition on Fe^{2+} [4]. As it follows from the results of this paper, the assignment of the band should rather be Fe^{2+}-V, with a photoionization threshold of 0.85 eV. A similar absorption band in the near IR is also known in $LiNbO_3$:Fe and has been commonly assigned to an intraion d-d transition on Fe^{2+}[Nb] [43]. Conversely, it was noted in Refs. [42,45] that the long-wavelength onset of the band in $LiNbO_3$:Fe is very close to the ionization threshold of Fe^{2+}[Nb] such that an absorption associated with photoionization of Fe^{2+}[Nb] may also be contributing. This is exactly what is observed in $KNbO_3$:Fe; compare the long-wavelength onset of absorption at ≈0.83 eV (≈1500 nm) with the ionization threshold of Fe^{2+}-V at 0.85 ± 0.01 eV (transition 1) found in this paper. We believe the striking similarity of the two systems is quite indicative, and the same conclusion should be made for $KNbO_3$:Fe; the near-IR absorption band is at least partially due to photoionization of Fe^{2+}-V. The situation may also be analogous to the case of dopant lanthanide ions where the $5d$ excited state is often found close to, or resonant with, the bottom of the CB; then excitation to the $5d$ state can be followed by delocalization of the $5d$ electron (generation of free electron in the CB) [46–49].

A novel feature of the spectra in Fig. 4(a) is the reduction-induced drop of absorption in the region from 390 nm (3.18 eV) to 430 nm (2.88 eV). The drop is better visualized in Fig. 4(b), which directly shows the effect of reduction by subtracting the absorption spectrum of the as-grown sample from the spectrum of the reduced sample. In view of the above-given EPR data, it is most natural to associate the observed decrease of the near-UV absorption with the decrease of the concentration of Fe^{3+}-V centers. Following again the interpretation for $LiNbO_3$:Fe, the absorption mechanism is then a phototransfer of an electron from the VB to Fe^{3+}-V (transition 2 in Fig. 2), often called "charge transfer" [45].

As shown in Fig. 1 (EPR data), electroreduction with gold electrodes virtually eliminated the EPR signal associated with Fe^{3+}-V complexes, leading to the expectation that the corresponding optical absorption in the near UV (electron transfer from the VB to Fe^{3+}-V, transition 2 in Fig. 2) would nearly vanish. Although a significant drop (factor of 2) occurs in the near UV (Fig. 4), the remaining absorption is just as strong as the broadband absorption in the visible region. As it is definitely associated with Fe (comparison with the absorption spectra of undoped samples in the literature: Ref. [4]), the remaining absorption can only be assigned to Fe^{3+}[Nb]: electron transfer from Fe^{3+}[Nb] to the CB, transition 3 in Fig. 2. Even in the case of strongly decreased concentration of Fe^{3+}-V, the unchanged concentration of Fe^{3+}[Nb] centers and potentially the oxygen vacancies would still be present as charge acceptors.

Four different absorption mechanisms (arrows 1, 2, 3, and 4 in Fig. 2) due to two physically different centers (Fe-V and Fe[Nb]) are superimposed in the optical absorption of $KNbO_3$:Fe. Unlike the case $LiNbO_3$:Fe, where pure spectra of each oxidation state, Fe^{2+} and Fe^{3+}, were obtained [42], reliable deconvolution of the absorption spectra of $KNbO_3$:Fe is not possible. Only estimations of the corresponding long-wavelength onsets could be made from the $KNbO_3$:Fe absorption spectra.

In principle, more information about individual absorption spectra for the participating electron transfer mechanisms could be found through a correlated study of photochromic absorption vs photochromic EPR. For example, such a method was successfully applied to $BaTiO_3$:Rh, see Ref. [50]. However, a photochromic EPR effect in our $KNbO_3$:Fe samples, either as-grown or reduced, was weaker than a small fraction of a percent when measured under optical irradiation conditions similar (Xe lamp with interference filters) to those used in Refs. [50,51]. Even the use of a much stronger irradiation (laser sources instead of Xe lamp with interference filters), hundreds of milliwatts per square centimeter, did not make a difference. No new lines nor noticeable changes to the intensities of the previously found EPR lines have been detected; therefore, there was simply no way to apply this technique to $KNbO_3$:Fe.

At the same time, individual absorption spectra and their long-wavelength onsets for all possible participating electron transfer mechanisms is a very important issue. Knowledge of the long-wavelength onsets (photon energy thresholds) together with the wavelength dependencies of the photoionization cross-sections would enable predictions of photorefractive properties at any particular wavelength and would facilitate the tailoring of the material properties to meet the needs of particular applications. Below, we compare the roles of different photoelectron transfer processes in the generation of electron and/or hole carriers in $KNbO_3$:Fe; this is evaluated for different spectral regions in the as-grown and reduced samples.

TABLE II. Photorefractive transitions in the as-grown and reduced samples. Minimum photon energies of 0.66 eV (for E_4) and 0.85 eV (for E_1) are required in the as-grown and reduced samples, respectively. Transitions in brackets denote the trapping for the free carriers by charge acceptors. The gray areas depict the energy regions where the transitions occur; the photon energy is increasing from left to right. $E_i (i = 1-4)$ correspond to the labels used in Fig. 2. This table does not include a $\mathrm{Fe}^{2+/3+}$[Nb] or oxygen vacancies (V_O) levels identified in Refs. [4,52], which both sit above the Fermi level and can trap electrons.

Photon energy		2.35 eV	2.54 eV
As-grown	$(E_4)\, h\nu + \mathrm{Fe}^{4+}[\mathrm{Nb}] \rightarrow \mathrm{Fe}^{3+}[\mathrm{Nb}] + h^+$ $\{h^+ + \mathrm{Fe}^{3+}[\mathrm{Nb}] \rightarrow \mathrm{Fe}^{4+}[\mathrm{Nb}]\}$		
Reduced	$(E_1)\, h\nu + \mathrm{Fe}^{2+}\text{-}V \rightarrow \mathrm{Fe}^{3+}\text{-}V + e^-$ $\{e^- + \mathrm{Fe}^{3+}\text{-}V \rightarrow \mathrm{Fe}^{2+}\text{-}V\}$		
As-grown		$(E_2)\, h\nu + \mathrm{Fe}^{3+}\text{-}V \rightarrow \mathrm{Fe}^{2+}\text{-}V + h^+$ $\{h^+ + \mathrm{Fe}^{3+}[\mathrm{Nb}] \rightarrow \mathrm{Fe}^{4+}[\mathrm{Nb}]\}$	
Reduced		$(E_2)\, h\nu + \mathrm{Fe}^{3+}\text{-}V \rightarrow \mathrm{Fe}^{2+}\text{-}V + h^+$ $\left\{\begin{array}{l} h^+ + \mathrm{Fe}^{2+}\text{-}V \rightarrow \mathrm{Fe}^{3+}\text{-}V \text{ and/or} \\ h^+ + \mathrm{Fe}^{3+}[\mathrm{Nb}] \rightarrow \mathrm{Fe}^{4+}[\mathrm{Nb}] \end{array}\right\}$	
As-grown			$(E_3)\, h\nu + \mathrm{Fe}^{3+}[\mathrm{Nb}] \rightarrow \mathrm{Fe}^{4+}[\mathrm{Nb}] + e^-$ $\left\{\begin{array}{l} e^- + \mathrm{Fe}^{4+}[\mathrm{Nb}] \rightarrow \mathrm{Fe}^{3+}[\mathrm{Nb}] \text{ and/or} \\ e^- + \mathrm{Fe}^{3+}\text{-}V \rightarrow \mathrm{Fe}^{2+}\text{-}V \end{array}\right\}$
Reduced			$(E_3)\, h\nu + \mathrm{Fe}^{3+}[\mathrm{Nb}] \rightarrow \mathrm{Fe}^{4+}[\mathrm{Nb}] + e^-$ $\{e^- + \mathrm{Fe}^{3+}\text{-}V \rightarrow \mathrm{Fe}^{2+}\text{-}V\}$

E. Photoelectron transfer in $\mathrm{KNbO_3}$:Fe: Reduction and wavelength dependence

There are four photon energy-dependent transitions that can in principle occur between Fe ions and host electron bands of $\mathrm{KNbO_3}$, as seen in Fig. 2 (arrows 1–4). These transitions contribute to optical absorption, photoconductivity, and photorefraction through the transfer of electrons from Fe^{2+}-V to CB (E_1), from VB to Fe^{3+}-$V(E_2)$, from Fe^{3+}[Nb] to CB (E_3), and from VB to Fe^{4+}[Nb] (E_4). Which of these transitions dominate in a particular sample under irradiation at a particular wavelength depends on the population of Fe levels in as-grown or reduced samples (see Table II).

As described in Sec. C, various transitions occur based on the particular charge (valence) states of the impurities available in a crystal. As-grown samples do not contain Fe^{2+}-V, and therefore transition 1 (photon energy threshold of 0.85 ± 0.01 eV) cannot occur; the corresponding broad band absorption in the visible and near IR is therefore absent. Fe^{4+}[Nb] are present, thus enabling transition 4 that generates holes in the VB (0.66 ± 0.04 eV threshold), which is typically broad and spanning from the near IR to UV. Such an absorption band is weak [shown in Fig. 4(a) (dashed line)], which is due to a very small amount of Fe^{4+}[Nb] in our samples. Nevertheless, this small amount is responsible for the holes generated in the VB and responsible for the photorefractive effect (hole-type) observed in as-grown crystals at long wavelengths [4]; this is the only photorefractive mechanism in as-grown samples for photon energies $\geqslant 0.66$ eV and <2.35 eV. For energies greater than $E_2 (\approx 2.35\,\mathrm{eV})$, a second hole-generating mechanism is activated, i.e. charge-transfer to the Fe^{3+}-V center, while for energies greater than E_3 (≈ 2.54 eV), electrons are generated due to photoionization of Fe^{3+}[Nb], resulting in electron-type photorefraction. In this latter case, both holes and electrons would play a competing role in the formation of the photorefractive grating.

Reduced samples contain Fe^{2+}-V, and therefore transition 1 occurs, resulting in a broad band absorption in the visible and near IR. With the absence of Fe^{4+}[Nb], holes are only generated at energies $>2.35\,\mathrm{eV}(E_2)$. Only electron-type photorefraction can occur in reduced samples for photon energies $\geqslant 0.85$ and <2.35 eV. For energies greater than $E_2 (\approx 2.35\,\mathrm{eV})$, a hole-generating mechanism is activated, i.e. charge-transfer to the Fe^{3+}-V center; although, at a slightly higher energy ($E_3 \approx 2.54\,\mathrm{eV}$), an additional source of electrons becomes available due to the photoionization of Fe^{3+}. The photon energy thresholds for these transitions are quite close to each other (≈ 2.35 and ≈ 2.54 eV), such that both types of photoconductivity (electrons and holes), and in turn both types of gratings (hole and electron), may simultaneously occur in the blue-green spectral region. Either type may be prevailing depending on the particular wavelength of irradiation and level of reduction. The impact of such dynamics for the desired electron photorefractive grating for reduced samples is that the competition between the electron and hole generated gratings is eliminated for energies <2.35 eV. For energies >2.35 eV, this competition is minimized in reduced samples with respect to as-grown samples because of the decreased concentration of hole-generating Fe^{3+}-V centers (i.e. transition 2 plays less of a role in reduced samples). Although this appears to be desirable, it could create another issue as it would minimize the electron acceptor population. However, the energy levels of Fe^{3+} (associated with the empty $\mathrm{Fe}^{2+/3+}$ level, dashed bars in Fig. 2) and isolated V_O centers described in Refs. [4,52] sit above the Fermi level and can be electron traps (see Fig. 2). Recall that the photorefractive effect requires both charge donor and acceptor states.

When adding up all participating processes for photon energies $\geqslant 2.54$ eV, the overall number of hole-contributing centers shown in Fig. 2 is less in reduced samples (2 electron-generating centers vs 1 hole-generating center) compared to as-grown samples (1 electron-generating center vs 2 hole-generating centers). In an ideal case, only one (main) center would be used in each material. In an as-grown sample, this would be the result of transition 4 (Fe^{4+}[Nb]), and in a reduced sample, it would be the result of transition 1 (Fe^{2+}-V). In this case, the electron-hole competition would be eliminated. For the reasons described in Sec. F, electron conductivity allows for an improved photorefractive response time in iron-doped $KNbO_3$.

Although Fe^{4+}[Nb] centers are absent in reduced samples in thermal equilibrium (in dark) as described above, they can be produced by irradiation with photon energies >2.54 eV through the photoionization of Fe^{3+}[Nb] (transition 3), resulting in Fe^{4+} and a free electron; this in turn provides another source of holes (transition 4). If this electron returns to the parent Fe^{4+}, which would occur in the case where the Fe^{3+} ions are below the Fermi level, then the lifetime of the Fe^{4+} ion is equal to the free carrier lifetime, and the electron does not contribute to the photorefractive effect (no buildup of a space-charge field). If the electron is trapped by another electron acceptor, then the Fe^{4+} ions can be long-lived and become an additional source of hole conductivity; therefore, a photon energy of $\approx$2.54 eV is an important margin where Fe^{4+}[Nb] may also begin to contribute to the electron-hole competition (i.e. competing gratings), even in a reduced sample. Note: the charge states of the centers are shown in thermal equilibrium in the dark (Fig. 2); Fe^{4+}[Nb] appears only in the energy level diagram for the as-grown samples (Fig. 2, left), whereas the reduced samples (Fig. 2, right) require light to create Fe^{4+}[Nb] ions. In contrast to the example above (reduced samples), as-grown samples inherently have Fe^{4+}[Nb], and any of these Fe^{4+}[Nb] ions can capture the electron ($e^- + Fe^{4+}[Nb] \rightarrow Fe^{3+}[Nb]$), thereby contributing to the space-charge field formation, see Table II. Similarly, a hole capture transition ($h^+ + Fe^{3+}[Nb] \rightarrow Fe^{4+}[Nb]$) would only cause photorefraction in an as-grown sample. The combination of these processes in the as-grown samples, which include both electron and hole capture centers, result in electron-hole competition. For these reasons, it is clear that as-grown samples are more susceptible to competing grating effects (i.e. less efficient beam coupling), more so than reduced samples.

Table II and Fig. 2 clearly illustrate that the presence of two physically different Fe centers (two charge states of each: $Fe^{3+/4+}$[Nb] and $Fe^{2+/3+}$-V) can cause a large variety of charge transfer processes. While Fig. 2 only labels the generation of free charges, Table II identifies charge generation, charge capture, and the corresponding charge state conversions of donor and acceptor centers. In Table II, only the transitions that provide the required charge separation, i.e. photo-induced free carrier generation and trapping of the free carriers, are shown.

F. Photorefractive effect in $KNbO_3$:Fe

To demonstrate the dramatic effect of hole or electron transitions on the response time and efficiency of dynamic holographic processes, two-beam coupling measurements were used. These measurements were conducted with a 532 nm (2.33 eV) laser to record dynamic gratings in a self-pumped reflection geometry (i.e. high resolution gratings). An individual crystal was chosen with a nonuniform reduction (reduced using Ag electrodes in air), such that part of it was a yellowish-green color (same appearance and optical absorption as an as-grown sample) and the other part was a brownish color (same appearance and optical absorption as a reduced sample). A map of the concentration of photoionizable centers of the crystal used in this paper can be found in Ref. [53]. This crystal was ideal for comparing the photorefractive effect resulting from unreduced and reduced Fe, without the concern of potential variations that could exist from crystal to crystal. For both cases of unreduced and reduced regions of the sample, 532 nm laser light activated the main photorefractive center of each region: Fe^{4+} (transition 4, holes) in the unreduced region and Fe^{2+}-V (transition 1, electrons) in the reduced region. Although 532 nm (2.33 eV) light is close to the energy required for transition 2, shown in Fig. 2, it is only at the threshold and does not have any significant contribution to the formation of the space-charge field/photorefractive grating in either region. A weak generation of holes from transition E_2 is more evident in the as-grown sample absorption spectrum [Fig. 4(a), dashed line], which is virtually zero absorption at 532 nm. This is more difficult to see in the absorption spectrum of a reduced sample because the same pure contribution of E_2 is masked by the larger E_1 contribution.

The most significant result observed is that the optical gain occurred in opposite directions when comparing these two regions; this is a direct consequence of the dominant type of photoconductivity, i.e. opposite sign charge carriers generated with 532 nm light in different regions. Furthermore, the response times of two-beam coupling can also be used to determine the dominant type of charge carrier in a given region. In the unreduced region, the two-beam coupling $1/e$ response time was $\approx$30 ms; in this case, 532 nm light activated transition E_4 (holes). In the reduced portion of the crystal (using the same power density), the $1/e$ response time was <100 μs; in this case, 532 nm light activated transition E_1 (electrons). The substantially faster response times (measured under the CW pumping) in the reduced regions of the crystal are due to two main reasons. First, the band mobility of electrons is at least 10 times as large as band mobility of holes in $KNbO_3$: see Refs. [4,54–56]. Although for small grating spacings (as is the case for the counterpropagating two-beam coupling geometry used in this paper), the effect of charge mobility tends to cancel out: see Eq. (16) in Ref. [9] (diffusion length in the equation is related to band mobility through the Einstein relation). The second reason is related to a much larger concentration of photoionizable centers (Fe^{2+}-V as a source of electrons compared to Fe^{4+} as a source of holes), which seems to be the dominant cause. This can be seen from Eqs. (9) and (16) in Ref. [9], where the rate of formation of the space-charge field is proportional to the concentration of photoionizable centers (i.e. absorption constant). Depending on reduction, the ratio of the absorption coefficients can be quite large, as shown in Fig. 4.

The photorefractive beam-coupling efficiency (i.e. change in optical density, $\Delta OD = \log(P_{in}/P_{out})$ between these two regions was also significantly different: $\Delta OD \approx 0.7$ in the unreduced region and 1.5 in the reduced region. It should be noted that, in this sample, the two different regions were nonuniformly "reduced" and "unreduced". Although this sample was ideal for showing the change in gain direction and the orders of magnitude difference in the response times, the difference in ΔOD was less pronounced than it would be in the ideal case using uniform as-grown samples and reduced crystals. For this reason, ΔOD was also measured on a separate uniformly reduced crystal (using Au electrodes in air). Here, the result was dramatically different: $\Delta\text{OD} \approx 2.5$. Incidentally, the $1/e$ response in the uniformly reduced sample was $\approx 50\ \mu$s.

IV. CONCLUSIONS

For the first time a comprehensive study of Fe associated defects has been accomplished comparing as-grown (unreduced) and reduced $KNbO_3$:Fe crystals. This investigation was only made possible by improvements to the electroreduction technique. Through the use of EPR results, it was determined that nonoxidizing electrodes are essential for a strong and homogeneous electroreduction process, not simply an oxygen-deficient atmosphere. Such modifications to this process allowed for the creation of charge donors in greater and more uniform concentrations. Due to the improved reduction process, this paper has determined the relative concentrations of the Fe centers (Fe and Fe-V) responsible for the various charge transitions that enable the photorefractive effect.

The mystery of the inconsistency of different authors over the years in terms of the nature of the defect structure in $KNbO_3$ has been resolved by showing that the different complex centers described in the past (Müller and Schirmer Groups, [19,21]) are actually the same center in *all* cases. Through the use of EPR, optical absorption, and electric conductivity measurements, various electron and hole donor states and corresponding charge acceptor states have been determined. In contrast to the previously used conventional model, the *main* photorefractive centers have been identified as the Fe^{2+}-V complex in reduced samples and Fe^{4+}[Nb] in as-grown samples.

The presence of two physically different Fe centers in comparable concentrations (each in two charge states: $Fe^{3+/4+}$[Nb] and $Fe^{2+/3+}$-V) provides a larger variety of electron transfer processes compared to the case of previously suggested models of a single Fe center that exists in several charge states ($Fe^{2+/3+}$ in $LiNbO_3$:Fe, and $Fe^{2+/3+}$,$Fe^{3+/4+}$ in $KNbO_3$:Fe). In the case of different centers, the creation of Fe^{2+}-V is not accompanied by a decrease of the Fe^{3+}[Nb] concentration, opposed to the one-center models where Fe^{2+} ions can appear under reduction only at the expense of a corresponding decrease of the Fe^{3+}[Nb] concentration. This is an important finding, as it allows for the creation of donors via electroreduction (field-assisted diffusion) without sacrificing the acceptor concentration.

An energy scheme of the Fe electronic levels in the bandgap of $KNbO_3$ has been constructed for the two charge states, $Fe^{2+/3+}$-V and $Fe^{3+/4+}$[Nb]. The location of $Fe^{2+/3+}$-V and $Fe^{3+/4+}$[Nb] electronic levels relative to the bottom of the CB and the top of the VB were determined (threshold energies for all four electronic transitions between the two Fe centers and the host electron bands were found). In addition, the absorption bands have been assigned to these specific transitions, particularly those that involve the Fe complexes that had not been previously considered. Different mechanisms of optical absorption and photoconductivity due to the four electronic transitions and their governing effect on photorefractivity have been determined for as-grown and reduced samples over a broad spectral range. This allows for the prediction of beam-coupling performance under different scenarios (e.g. electron, hole, or electron-hole competing gratings) and provides the insight to engineering an advanced photorefractive crystal.

As a tool for determining dynamic holographic performance, beam-coupling measurements were employed to demonstrate the effects of pure-electron vs pure-hole gratings on the response (grating recording) times and beam-coupling efficiencies. The controlled formation and increased concentration of the Fe^{2+}-V center (electron donor center) as a result of the improved electroreduction method provided a dramatic enhancement to photorefractive performance over a broad spectral range (e.g. nearly 1000× faster response and significantly stronger beam-coupling efficiency).

This understanding of the isolated and complex centers involved in the dynamics of charge generation/trapping in $KNbO_3$:Fe provides better insight of what type of defect structure is required for the photorefractive effect. The identification of the main photorefractive centers (Fe^{4+}[Nb] in as-grown samples and Fe^{2+}-V in reduced samples) may allow for the modification of either the growth or the postgrowth processes to uniformly increase and control the concentration of the desired centers. This knowledge that enables the development of advanced materials for dynamic holographic applications may also be transferred to other materials classes.

ACKNOWLEDGMENTS

The authors would like to thank Dr. Gary Cook, Prof. Larry Halliburton, Prof. Partha Banerjee, and Prof. Ivan Biaggio for their valued input to this work.

---

[1] L. Hesselink, J. Feinberg, and G. Roosen, J. Phys. D: Appl. Phys. **41**, 220301 (2008).

[2] M. Zgonik, C. Medrano, M. J. Ewart, H. Wuest, and P. Guenter, Opt. Eng. **34**, 1930 (1995).

[3] C. Medrano, E. Voit, P. Amrhein, and P. Günter, J. Appl. Phys. **64**, 4668 (1988).

[4] M. Zgonik, M. Ewart, C. Medrano, and P. Günter, in *Photorefractive Materials and Their Applications 2*, edited by P. Günter and J.-P. Huignard, Springer Series in Optical Sciences (Springer, New York, 2007), Vol. 114, Chap. 7.

[5] D. R. Evans, G. Cook, J. L. Carns, M. A. Saleh, S. A. Basun, J. M. Seim, and G. J. Mizell, Opt. Lett. **31**, 89 (2006).

[6] G. Cook, J. L. Carns, M. A. Saleh, and D. R. Evans, Phys. Rev. B **73**, 174102 (2006).

[7] R. Rebhi, P. Mathey, H. R. Jauslin, S. Odoulov, G. Cook, and D. R. Evans, Opt. Lett. **34**, 377 (2009).

[8] P. Mathey, H.-R. Jauslin, G. Gadret, G. Cook, D. R. Evans, and S. Odoulov, J. Opt. Soc. Am. B **27**, 1481 (2010).

[9] P. Günter, Phys. Rep. **93**, 199 (1982).

[10] E. Voit, M. Z. Zha, P. Amrhein, and P. Günter, Appl. Phys. Lett. **51**, 2079 (1987).

[11] J. O. White and A. Yariv, Appl. Phys. Lett. **37**, 5 (1980).

[12] B. Kippelen, S. N. Peyghambarian, S. R. Lyon, A. B. Padias, and H. K. Hall Jr., Electron. Lett. **29**, 1873 (1993).

[13] P. Buranasiri, P. P. Banerjee, V. Polejaev, and C. C. Sun, Proc. SPIE **5206**, 215 (2003).

[14] P. P. Banerjee, H.-L. Yu, D. A. Gregory, and N. Kukhtarev, Opt. Laser Technol. **28**, 89 (1996).

[15] A. E. T. Chiou and P. Yeh, Opt. Lett. **10**, 621 (1985).

[16] P.-A. Blanche, A. Bablumian, R. Voorakaranam, C. Christenson, W. Lin, T. Gu, D. Flores, P. Wang, W.-Y. Hsieh, M. Kathaperumal, B. Rachwal, O. Siddiqui, J. Thomas, R. A. Norwood, M. Yamamoto, and N. Peyghambarian, Nature **468**, 80 (2010).

[17] D. R. Evans and G. Cook, Laser Focus World, Dec. 12, 67 (2005).

[18] E. Siegel, Ph.D. thesis, University of Karlsruhe, 1974.

[19] E. Siegel, W. Urban, K. A. Mueller, and E. Wiesendanger, Phys. Lett. A **53**, 415 (1975).

[20] F. M. Michel-Calendini, M. Peltier, and F. Micheron, Solid State Commun. **33**, 145 (1980).

[21] E. Possenriede, O. F. Schirmer, H. J. Donnerberg, and B. Hellermann, J. Phys.: Condens. Matter **1**, 7267 (1989).

[22] S. Torbrügge, M. Imlau, B. Schoke, C. Merschjann, O. F. Schirmer, S. Vernay, A. Gross, V. Wesemann, and D. Rytz, Phys. Rev. B **78**, 125112 (2008).

[23] B. Briat, V. G. Grachev, G. I. Malovichko, O. F. Schirmer, and M. Wöhlecke, in *Photorefractive Materials and Their Applications 2*, edited by P. Günter and J.-P. Huignard, Springer Series in Optical Sciences (Springer, New York, 2007) Vol. 114, Chap. 2.

[24] U. Flückiger and H. Arend, J. Cryst. Growth **43**, 406 (1978).

[25] P. Amrhein, Ph.D. thesis, ETH Zürich, 1992.

[26] A. Krumins and P. Günter, Appl. Phys. **19**, 153 (1979).

[27] P. Günter, Ferroelectrics **22**, 671 (1978).

[28] P. Günter and F. Micheron, Ferroelectrics **18**, 27 (1978).

[29] D. R. Evans, G. Cook, J. L. Carns, M. A. Saleh, S. A. Basun, J. M. Seim, and G. J. Mizell, J. Lumin. **119–120**, 535 (2006).

[30] A. W. Hewat, J. Phys. C: Solid State Phys. **6**, 2559 (1973).

[31] E. Wiesendanger, Ferroelectrics **6**, 263 (1973).

[32] B. Zysset, I. Biaggio, and P. Günter, J. Opt. Soc. Am. B **9**, 380 (1992).

[33] D. R. Evans, S. A. Basun, M. A. Saleh, A. S. Allen, T. P. Pottenger, G. Cook, T. J. Bunning, and S. Guha, IEEE J. Quantum Electron. **38**, 1661 (2002).

[34] A. Abragam and B. Bleaney, *Electron Paramagnetic Resonance of Transition Ions* (Dover Publications, New York, 1986).

[35] E. S. Kirkpatrick, K. A. Müller, and R. S. Rubins, Phys. Rev. **135**, A86 (1964).

[36] W. C. Wong, D. S. McClure, S. A. Basun, and M. R. Kokta, Phys. Rev. B **51**, 5682 (1995).

[37] M. Ewart, Ph.D. thesis, ETH Zürich, 1998.

[38] V. Gopalan, K. L. Schepler, V. Dierolf, and I. Biaggio, in *The Handbook of Photonics*, 2nd ed., edited by M. C. Gupta and J. Ballato (CRC Press, Boca Raton, FL, 2006), Chap. 6.

[39] G. Montemezzani and P. Günter, J. Opt. Soc. Am. B **7**, 2323 (1990).

[40] J. Tauc, R. Grigorovici, and A. Vancu, Phys. Status Solidi B **15**, 627 (1966).

[41] H. Kurz, E. Krätzig, W. Keune, H. Engelmann, U. Gonser, B. Dischler, and A. Räuber, Appl. Phys. (Berlin) **12**, 355 (1977).

[42] S. A. Basun, D. R. Evans, T. J. Bunning, S. Guha, J. O. Barnes, G. Cook, and R. S. Meltzer, J. Appl. Phys. **92**, 7051 (2002).

[43] M. G. Clark, F. J. DiSalvo, A. M. Glass, and G. E. Peterson, J. Chem. Phys. **59**, 6209 (1973).

[44] H. J. Reyher, N. Hausfeld, and M. Pape. J. Phys.: Condens. Matter **12**10599 (2000).

[45] S. A. Basun, G. Cook, and D. R. Evans, Opt. Express **16**, 3993 (2008).

[46] W. M. Yen, M. Raukas, S. A. Basun, W. van Schaik, and U. Happek, J. Lumin. **69**, 287 (1996).

[47] P. Dorenbos, J. Lumin. **91**, 155 (2000).

[48] C. W. Thiel, H. Cruguel, H. Wu, Y. Sun, G. J. Lapeyre, R. L. Cone, R. W. Equall, and R. M. Macfarlane, Phys. Rev. B **64**, 085107 (2001).

[49] E. van der Kolk, P. Dorenbos, C. W. E. van Eijk, S. A. Basun, G. F. Imbusch, and W. M. Yen, Phys. Rev. B **71**, 165120 (2005).

[50] M. Meyer, O. F. Schirmer, and R. Pankrath, Appl. Phys. B **79**, 395 (2004).

[51] H. Kröse, R. Scharfschwerdt, A. Mazur, and O. F. Schirmer, Appl. Phys. B **67**, 79 (1998).

[52] I. Biaggio, M. Zgonik, and P. Günter, Opt. Commun. **77**, 312 (1990).

[53] A. Regmi, Ph.D. thesis, Lehigh University, 2012.

[54] M. Ewart, I. Biaggio, M. Zgonik, and P. Günter, Phys. Rev. B **49**, 5263 (1994).

[55] I. Biaggio, M. Zgonik, and P. Günter, J. Opt. Soc. Am. B **9**, 1480 (1992).

[56] M. Ewart, M. Zgonik, and P. Günter, Opt. Commun. **141**, 99 (1997).